Stark dynamics of two-electron atoms probed by scaled energy spectroscopy

J. Murray-Krezan, J. Kelly, M. R. Kutteruf, and R. R. Jones
Department of Physics, University of Virginia, Charlottesville, Virginia 22904-4714, USA
(Received 14 September 2006; published 2 January 2007)

Orbital dynamics in two-electron alkaline earth atoms in a static electric field are studied using scaled-energy recurrence spectroscopy. Photoabsorption spectra for Ba and Ca Rydberg atoms are measured as continuous functions of static electric field and energy. In both Ba and Ca the laser excitation proceeds through the singly excited *nd* series which is strongly perturbed by doubly excited valence configurations. Clear signatures of the two-electron dynamics associated with these perturbing configurations are identified.

DOI: 10.1103/PhysRevA.75.013401 PACS number(s): 32.60.+i, 32.80.Rm, 39.30.+w

I. INTRODUCTION

Nearly two decades ago, Eichmann *et al.* [1] introduced scaled-energy recurrence spectroscopy (SERS) as a technique for revealing the semiclassical dynamics that underly complex energy spectra. Since that time, the method has been used in conjunction with closed-orbit theory [2], to explore the behavior of Rydberg atoms in the presence of strong electric and/or magnetic fields [1–13]. For example, for singly excited atoms in a static electric field F, SERS reveals the predominant time scales associated with (i) the motion of the electron along nearly closed Kepler ellipses with a characteristic period $\tau_K=2\pi n^3$, (ii) the precession of orbital angular momentum in the field with a Stark period, $\tau_S=2\pi/3Fn$, and (iii) scattering between uphill and downhill orbit configurations in nonhydrogenic atoms. Unless otherwise noted, atomic units are used throughout.

Given the substantial success in applying these experimental and computational methods to single-electron systems, it is not unreasonable to consider whether similar frequency domain techniques can be used to explore two-electron dynamics in the presence of external fields. Indeed, a framework for incorporating closed-orbit theory insight into a multichannel quantum-defect formalism has been established [5]. Yet in spite of the fact that a number of SERS experiments have focused on two-electron or multielectron systems [8–13], only one experiment in Ba [9] has utilized the method to focus exclusively on the role of configuration interaction in Stark dynamics within multielectron atoms.

In that experiment, Bates *et al.* [9] used direct laser excitation of the $5d7d\ ^1D_2$ perturber, which is embedded in, and coupled to, the singly excited $6snd$ Rydberg series in Ba. SERS and direct Fourier transform spectroscopy were used to interpret absorption spectra collected as a function of binding-energy and electric-field strength. A longer Kepler period than is observed in single-electron systems at the same binding energy was identified. This longer period was attributed to both the time lag associated with electron scattering back and forth between doubly and singly excited configurations and to an increased anharmonicity in the effective binding potential at energies near the perturber. Unfortunately, the range of electron binding energies that could be explored was restricted to the width of the $5d7d$ perturber. Thus the temporal resolution of the measurements was limited to the inverse of the resonance width, comparable to the time shifts that were inferred.

Here we examine Stark dynamics in the presence of strong configuration interaction from the perspective of the Rydberg rather than the valence configuration. We directly excite the Ca $4snd$ and Ba $6snd$ Rydberg series and record photoabsorption maps as continuous functions of electric field and electron binding energy. Embedded (see Fig. 1) in the Ca and Ba Rydberg series are the $3d3d$ [14] and $5d7d$ [17] perturbers, respectively. We explicitly compare and contrast the scaled-energy recurrence spectra obtained from different energy windows within the Stark maps, i.e., regions within or near the doubly excited resonances and regions not strongly influenced by these perturbers. This analysis allows us to identify clear signatures of the two-electron dynamics and characterize the general effectiveness of scaled-energy recurrence spectroscopy in revealing those dynamics.

II. EXPERIMENTAL PROCEDURE

The experimental apparatus has been described in detail previously [6]. Alkaline earth atoms, Ba or Ca, in a thermal beam are laser excited to Rydberg Stark states in a spatially inhomogeneous static electric field. The Rydberg atoms autoionize following an isolated core excitation of the valence electron, and produce an ion signal that is proportional to the Rydberg photoabsorption probability. An imaging detector allows us to distinguish between ions produced at different locations in the interaction region, enabling us to record Stark spectra as a continuous function of Rydberg energy and electric-field strength. These spectra are then transformed into scaled-energy recurrence maps.

For Ca, dye lasers with wavelengths 422 and 391–395 nm drive the transitions $4s4s\ ^1S_0 \rightarrow 4s4p\ ^1P_1$ and $4s4p\ ^1P_1 \rightarrow 4snd\ ^1D_2$ $(13<n<24)$. For Ba, the two-step excitation $6s6s\ ^1S_0 \rightarrow 6s6p\ ^1P_1 \rightarrow 6snd\ ^1D_2$ $(14<n<50)$ is

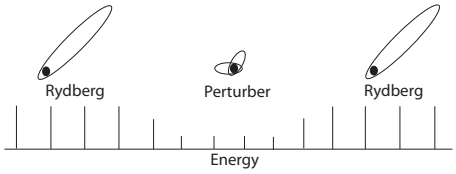

FIG. 1. Schematic diagram of a perturbed Rydberg series. The doubly excited perturber is embedded in the singly excited Rydberg series causing oscillator strength and quantum-defect variations.

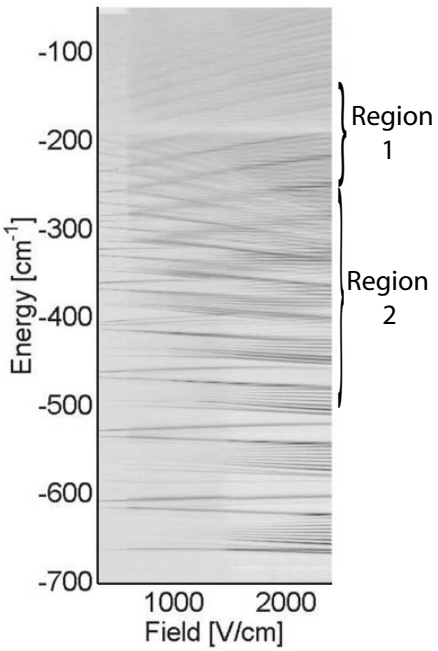

FIG. 2. Density plot of the measured Ba Stark map. Dark regions indicate large photoabsorption probability. The signal attenuation near $E=-194$ cm^{-1} (Region 1), is due to the $5d7d\ ^1D_2$ perturber. States at lower energy (Region 2) are not strongly affected by this perturber.

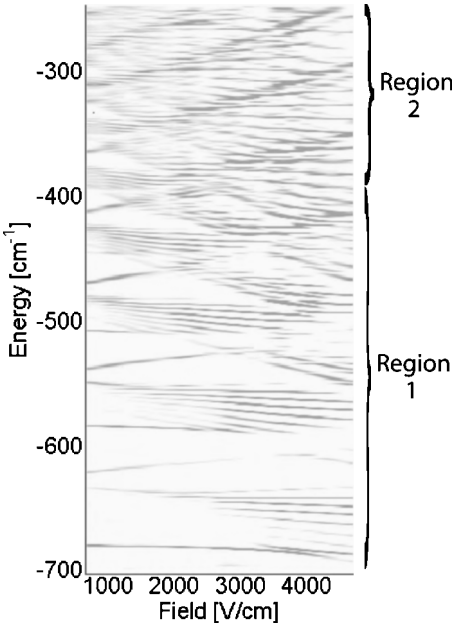

FIG. 3. Density plot of the measured Ca Stark map. Large photoabsorption probability is shown as dark regions. States in Region 1 are strongly coupled to the $3d3d$ perturber, while states in Region 2 are not.

performed using two dye lasers with wavelengths of 554 and 420–430 nm. Relative frequency calibration within the Rydberg spectrum is achieved to better than 0.3 cm^{-1} by monitoring the transmission of the second laser through a 2 cm solid étalon. The absolute frequency of the second laser is established to an accuracy better than 1 cm^{-1}, using the known positions of *nd* Rydberg states in zero field [14,17]. The laser-atom interaction region is defined from above by an aluminum plate and from below by 12 parallel wires that lie in a horizontal plane. The wires are spaced 2 mm from each other and 1.5 cm below the upper plate. A constant voltage difference between the wires is maintained using a resistor chain. The magnitude of the electric-field gradient in the interaction region is determined by the voltages applied to the two ends of the resistor chain. The voltage difference across the wires is always less than 5 kV to ensure electric-field gradient linearity and minimize nonvertical field components. The frequency of the second laser is scanned with fixed voltages applied across the ends of the resistor chain. Complete Stark maps are composites of the laser scans taken for different ranges of electric field.

Ten nanoseconds after the Rydberg excitation, a third dye laser excites electrons to an autoionizing state with near-unit efficiency, producing a position-dependent ion current proportional to the number of Rydberg atoms present at each point in the laser-atom interaction region. In Ca, 393 nm photons saturate the $4s^+ \rightarrow 4p^+_{3/2}$ transition. In Ba, the $6s^+ \rightarrow 6p^+_{3/2}$ transition is saturated with 455 nm photons. Ions produced at different locations within the spatially inhomogeneous electric field are projected through a 1.6 mm $\times$25 mm slit in the upper plate onto a MCP detector backed by a phosphor anode. The long dimension of the slit is perpendicular to the 12 wires that are responsible for the inhomogeneous field. Following each laser shot, the position-dependent fluorescence from the phosphor is imaged by a CCD camera and recorded using a frame grabber. Electric field versus position is calibrated by recording, as a function of laser frequency, the location of the static field-ionization threshold in the inhomogeneous field.

Spectroscopic data are compiled into Stark maps, as shown for Ba and Ca in Figs. 2 and 3, respectively. The Ba Stark map shows a pronounced window resonance, the $5d7d$ perturber, near $E=-194$ cm^{-1}. This perturber and its effect on the $6snd$ series has been studied previously in zero field [16,17] and in static electric fields [9,18]. The resonance spans approximately four n states, coupling singlet and triplet d-states with the perturber. At lower ($n<22$) and higher ($n>31$) energies the quantum defects of singlet and triplet d states do not vary significantly. However, near the perturber the quantum defects change rapidly [17].

In the Ca Stark map the effect of the $3d3d$ perturber is somewhat subtle. Its presence is more obvious in the zero-field spectrum shown in Fig. 4(a). Notably, the $4s15s$ state, located at $E=-685$ cm^{-1}, has a larger photoabsorption probability than the neighboring $4s14d$ state. However, for higher n values ($n \gg 20$) the spectrum follows the standard propensity rule for significantly stronger d, rather than s, excitation strength [19]. Armstrong *et al.* [14] observed a minimum in the d-state oscillator strength near $4s13d$ and Fig. 4(a) shows a clear attenuation of the d-state photoabsorption probability at energies, $E<-500$ cm^{-1}. In addition to oscillator strength variation, the quantum defect changes as a function of energy from $\delta_d=0.60$ at $n=13$ to $\delta_d=1.01$ at $n=22$.

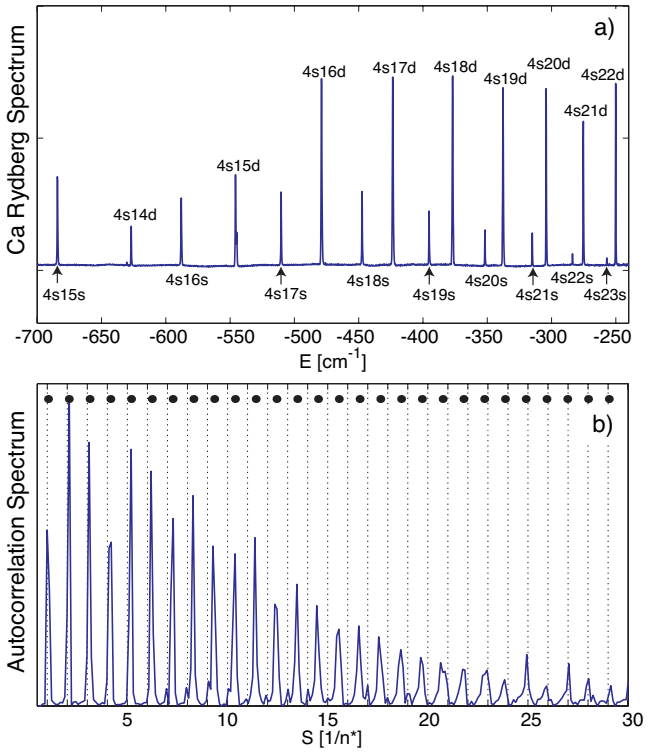

FIG. 4. (Color online) (a) Rydberg photoexcitation and (b) associated autocorrelation spectra of Ca. The 4*snd* Rydberg series is perturbed by the doubly excited 3*d*3*d* state. The autocorrelation spectrum shows the Rydberg character near the ion core as a function of action. Dashed lines at integer action mark the single-electron Kepler recurrences. Bullets (●) show the predicted peak positions when the variation in the quantum defect per n state, $\Delta\delta = 0.037$, is taken into account.

III. PRELIMINARY DISCUSSION

In our frequency-domain experiments in Ba and Ca, lasers populate Rydberg states from tightly bound, singly excited intermediate $6s6p\ ^1P_1$ and $4s4p\ ^1P_1$ levels, respectively. Dipole selection rules and radial wave-function overlap between the initial and final states ensure that the p electron is excited near the nucleus with a transition probability that is proportional to the singlet *nd* or *ns* Rydberg character at a given final-state energy.

The Fourier transform of the frequency-domain excitation spectrum is the temporal autocorrelation of an evolving wave packet [9,16]. This wave packet is not actually produced in the experiment, but it corresponds to what *would have been produced* if the atoms had been exposed to a short laser pulse with uniform spectral phase and a bandwidth spanning the range of energies included in the Fourier transform. The wave-packet autocorrelation function or recurrence spectrum $R(t)$ gives the overlap between the original wave packet (a d or s wave near the nucleus) and what it has become a time t later, thereby revealing natural time scales in the system. By changing the central energy and/or bandwidth of the sampling window before Fourier transforming, one can explore the characteristic energy dependence of the relevant wave-packet dynamics from a single frequency-domain spectrum.

Consider the Rydberg excitation spectrum for a single-electron atom in zero electric field. As derived directly from the energy spectrum, $R(t)$ is a rather complicated function, but the general features are well understood [20]. At early times, $R(t)$ shows large amplitude peaks separated by the Kepler period corresponding to the average electron energy in the excitation spectrum. Since the Rydberg electron is launched from the nucleus, these peaks represent returns of the wave packet to the vicinity of the ion. The Kepler modulations collapse and revive due to the nonuniform level spacing in the frequency spectrum. At times between these full revivals, smaller amplitude revival structures with periods that are integer fractions of the Kepler period are visible. The detailed appearance of $R(t)$ depends on the average energy and the range of energies included in the Fourier transform.

A much simpler time-domain spectrum can be generated by rescaling the independent axis in the excitation spectrum from binding energy E to principal quantum number $n^* = 1/\sqrt{2E}$ prior to Fourier transforming [6]. The scaled recurrence spectrum $R'(S)$ so obtained, shows a regular pattern of peaks appearing at integer values of action, S. $R'(S)$ measures the overlap of the evolving wave packet with its initial configuration, as a function of the number of orbits that it has completed, *independent of the Kepler period*. In a single-electron atom, the wave packet returns to its original configuration once on every orbit regardless of energy. As a direct consequence of the uncertainty principle, the Kepler recurrence peaks broaden as fewer n states are sampled. However, in contrast with the unscaled recurrence spectrum $R(t)$, *the peak positions in* $R'(S)$ *are totally independent of the average energy*, E_0, *and range of energies*, ΔE, *included in the Fourier transform*. The presence of two different angular momentum series in absorption spectrum (e.g., the *ns* and *nd* series in our measurements) affects the amplitudes of adjacent recurrence peaks. However, as long as the quantum defects of the series are constant, the recurrence peaks in $R'(S)$ always appear at integer action.

The situation is more interesting in two electron atoms where singly excited Rydberg series are coupled to tightly bound, doubly excited valence states resulting in energetically localized quantum-defect and oscillator-strength variations [19]. In this case, rescaling the binding-energy axis in an absorption spectrum from E to n^* does not produce a series of equally spaced absorption peaks. The associated modifications to the scaled recurrence spectra can be attributed to electron scattering between Rydberg and valence configurations during each return of the Rydberg electron to the ion core. Importantly, deviations from single-electron recurrence spectra are only observed if absorption spectra in the energetic vicinity of the perturber are included in the Fourier transform. Thus, in contrast to the single-electron case, $R'(S)$ depends critically on E_0 and ΔE, reflecting the energy-dependent two-electron dynamics.

For example, the scaled recurrence spectrum obtained from the zero-field Ca 4*snd* absorption spectrum at energies near the 3*d*3*d* resonance [Fig. 4(a)] is shown in Fig. 4(b). Peaks in $R'(S)$ mark the electron's return to the core as a d wave or s wave, but the d-wave contribution dominates. The nonconstant d-state quantum defect, caused by the coupling

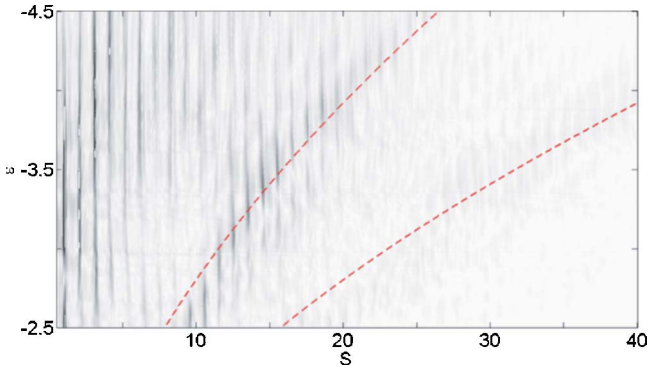

FIG. 5. (Color online) Ba recurrence map. Dashed lines mark the single-electron $j=1$ and 2 Stark revivals.

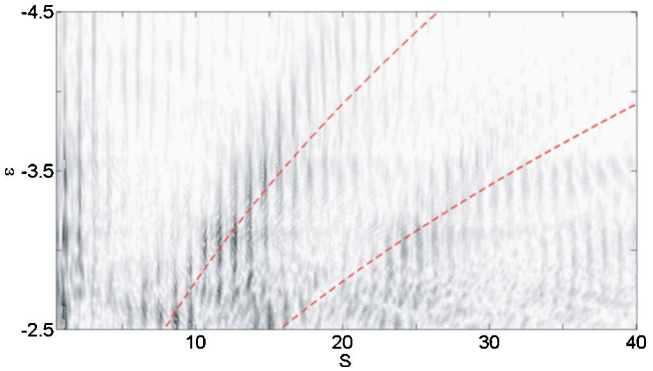

FIG. 6. (Color online) Ca recurrence map. Dashed lines mark the single-electron $j=1$ and 2 Stark revivals.

between the $4snd$ and $3d3d$ states, leads to a longer effective orbital period $\tau_K' \approx \tau_K(1+\Delta\delta_d)$, where $\Delta\delta_d \ll 1$ is the change in quantum defect per n state. At these energies, the electron scatters into and back out of the perturber configuration once during each Kepler period. The time spent in the doubly excited state adds to the recurrence time so that near the $3d3d$ perturber the characteristic orbital recurrence in Ca becomes $S_K' \approx S_K(1+\Delta\delta_d)$. Although $\Delta\delta_d$ is only a few percent, after several orbital periods, the extra time accumulates and the electron returns to the core significantly after the standard Kepler recurrence. The additional time per orbital period is spent near the atomic core [15].

To reveal the periodic orbital dynamics of a hydrogenic atom in a static electric field, a Stark map of absorption probability vs field vs binding energy, can be converted to scaled units, absorption probability vs scaled energy $\epsilon = E/\sqrt{F}$ vs n^* [6] and Fourier transformed with respect to n^*, to produce a scaled-energy recurrence map, $R'(S,\epsilon)$. Analogous to the zero-field case, the recurrence strength at each point (S,ϵ) is proportional to the probability that an electron wave packet, launched from the ion core at $t=0$ with scaled energy ϵ, has returned to the core in its initial configuration at a time S later. However, because of the static field, a characteristic time scale other than the Kepler period appears [6,9,20]. The electric field subjects the orbiting electron to a torque, so orbital angular momentum is not conserved. Instead an electron launched from the vicinity of the nucleus has a time-dependent angular momentum L, which evolves from low to high and back to low values at a characteristic, scaled-energy-dependent Stark period. Since an electron with high L has a negligible probability of approaching its initial launch point near the nucleus, strong Kepler recurrences are not visible during the fraction of the Stark period when the electron has high L. Because of the Stark precession, electron returns occur at integer (half-integer) action following an even (odd) number of Stark periods [6]. Yet in spite of the fact that the scaled-energy-dependent dynamics are more complex than in the zero-field limit, aside from uncertainty principle limits on resolution, the scaled-energy recurrence maps in hydrogenic atoms are independent of the values of E_0 and ΔE used in the Fourier transform.

In nonhydrogenic, single active-electron atoms the presence of additional electrons in the ion core adds a binding-energy-dependent term to the scaled one-electron Hamiltonian. This term is responsible for the avoided level crossings that appear in the Stark map [19] and associated "core-scattered" peaks in the recurrence spectrum [7]. The core-interaction term affects the fine-scale cross-section modulations associated with the Stark-level structure corresponding to a given n state, but strong variations in oscillator strength as the energy is scanned over each n manifold remain. Due to nonhydrogenic core scattering, $R'(S,\epsilon)$ acquires a dependence on the average energy E_0 and range of energies ΔE used in the Fourier transform. However, it is primarily the amplitudes of the recurrence peaks, not their locations, that are affected [12]. Thus, we can analyze the perturbed Ba and Ca Stark spectra with SERS and associate the energy-dependent recurrence peak shifts, broadening, and splittings (which are not seen in single-electron spectra) with two-electron effects.

IV. EXPERIMENTAL RESULTS

Figures 5 and 6 are the Ba and Ca recurrence maps, respectively. The coarse structures in the maps are strikingly similar to those associated with single-electron atoms. This is perhaps surprising in light of the strong perturbations in the Rydberg and Stark spectra of these two-electron systems. Dark vertical stripes near integer and half-integer values of S mark the Kepler motion of the electron. The maps also clearly illustrate the variation in the angular momentum precession rate as a function of scaled energy. For large negative values of ϵ, the electric field is relatively weak and many Kepler recurrences are observed before the electron's increasing angular momentum temporarily precludes further returns to the vicinity of the nucleus. Conversely, for less negative ϵ, the angular momentum precession from low to high and back to low l configurations occurs more rapidly. Accordingly, bands (or sequences [10]) of recurrence maxima are observed centered on the Stark recurrence times,

$$S_j = \left(\frac{4}{3}\epsilon^2 - \frac{1}{2}\right)j, \tag{1}$$

for the jth repetition of the Stark period. In single-electron systems, recurrence maxima within the jth-band appear at integer (half-integer) values of S for even (odd) values of j [6].

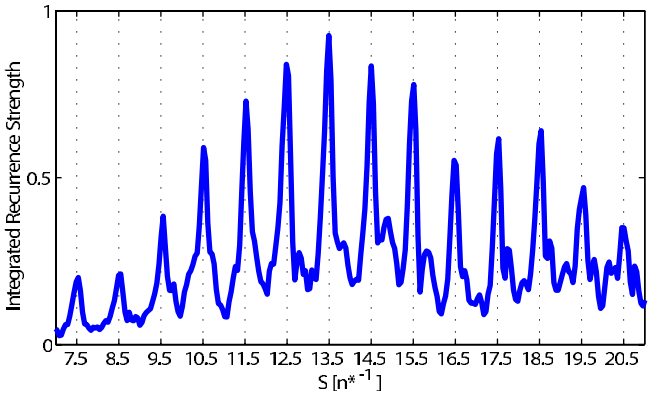

FIG. 7. (Color online) Recurrence strength in the first sequence in Ba integrated over scaled energy as a function of action. The shoulders and splitting of the primary recurrences are signatures of two-electron dynamics associated with the $5d7d$ perturber. The light vertical lines mark the positions of the single-electron recurrences, which occur at half-integer values of the action.

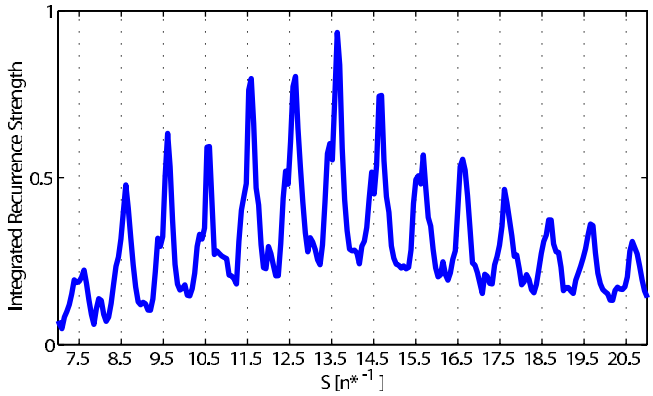

FIG. 8. (Color online) Strength of the first sequence of Ca recurrences integrated over scaled energy as a function of action. The shifts and fine-structure of the Ca peaks reflect the 2-electron dynamics associated with the $3d3d$ perturber. The light vertical lines mark the positions of the single-electron recurrences, which occur at half-integer values of the action.

In the Ba recurrence map the first Stark revival is clearly visible but the recurrences in the second revival are weak. Within the first sequence, clear recurrence maxima are observed at half-integer values of S, as in the single-electron case [6]. However, the recurrence peaks exhibit shoulders and subsidiary maxima, which are not seen in analogous one-electron systems. This fine structure is more apparent in Fig. 7, where the recurrence strengths of the $j=1$ sequence are integrated over ϵ at constant action. This condensed representation of the recurrence signal shows the return of the wave packet to the ion core, following a single Stark precession, as a function of the Stark period. This view is particularly useful for revealing the two-electron dynamics and is readily derived from our experimental recurrence maps. As noted above and discussed in more detail in Sec. V, the fine structure of the recurrence peaks is a direct result of the electron-electron interaction near the ion core.

In Ca, we find similar, though not identical behavior. For example, sequences corresponding to both the first and second Stark revivals are clearly visible. In Fig. 8, we plot the recurrence spectra in the $j=1$ sequence integrated over ϵ at constant action. As in the Ba data, fine structure on the primary recurrence peaks is clearly visible. In contrast with the Ba spectra, the primary recurrence maxima in the first sequence in Ca are shifted relative to half-integer values. These deviations are particularly visible at large action. Similar, albeit larger, shifts are observed in the zero-field autocorrelation in Ca [see Fig. 4(b)], and are the result of configuration interaction.

V. DISCUSSION

As noted in Sec. III, when generating a scaled recurrence spectrum, the range of energies ΔE included in the Fourier transform sets the effective excitation bandwidth for a particular wave packet. Producing this wave packet would require a laser pulse with a duration $\tau_L \sim 1/\Delta E$. Since an electron promoted to a Rydberg state near the nucleus leaves the vicinity of the nucleus in a few femtoseconds, the spatial extent of the wave packet immediately following the launch pulse is larger for smaller values of ΔE. The recurrence spectrum is a measure of the similarity between this initial wave packet and itself at a time S later. In a two-electron system, the situation is more complicated. If ΔE spans a perturbing resonance, the laser creates an outgoing Rydberg electron in a singly excited configuration (ns and nd in our experiments). However, this electron can scatter from, and exchange energy with, a valence electron in the ion core, creating a tightly bound doubly excited state [16,21]. Part of the wave packet remains in the Rydberg configuration and rapidly moves away from the nucleus. The doubly excited portion of the wave packet eventually decays, via electron-electron scattering, back into the Rydberg channel. The scattering occurs with a lifetime τ_{AI} and, provided the energy width $\Gamma \sim 1/\tau_{AI}$ of the perturbing resonance spans at least two Rydberg states, the process is essentially identical to autoionization [21]. The only difference being that following the decay, the outgoing Rydberg electron does not have sufficient energy to leave the atom and will eventually return to the nucleus sometime after one Kepler orbit of the Rydberg electron. For finite excitation bandwidths overlapping perturbing resonances, immediately following the launch pulse, the wave packet has both Rydberg and perturber character. Moreover, because of interference of Rydberg waves that promptly leave the ion core with those that spend some time in the doubly excited configuration, the Rydberg part of the wave packet can have a complex spatial structure at the end of the launch pulse. These interferences and configuration mixing are the source of the Kepler recurrence peak shifts and fine structure seen in the Ba and Ca data (see Figs. 7 and 8).

Of course, the precise recurrence structures that are observed depend on the details of the effective wave packet that is launched. E_0 and ΔE can be chosen at will to alter the spatial distribution and electron configuration of the wave packet whose evolution is revealed in the recurrence spectrum. Accordingly, we take advantage of the continuous

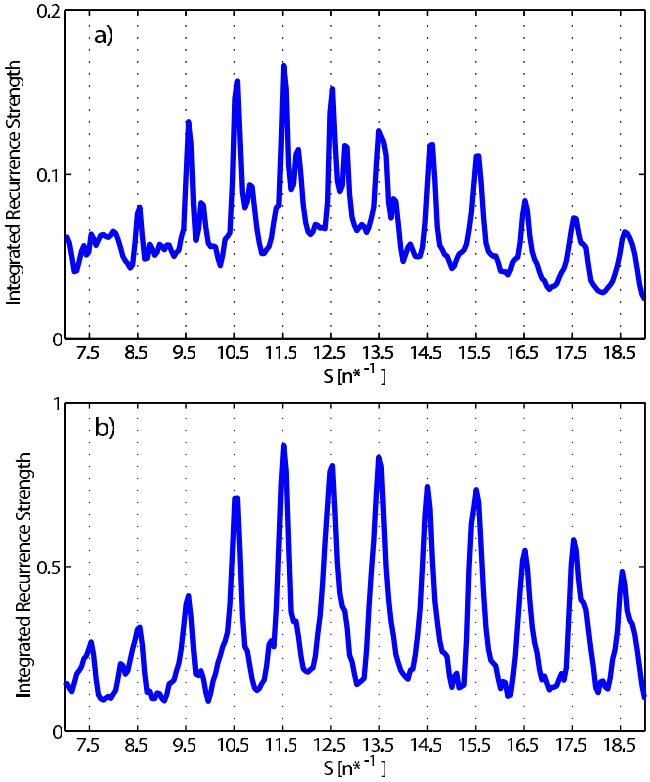

FIG. 9. (Color online) Integrated first-recurrence sequence in Ba sampled in two different energy windows. (a) is taken from region 1 in Fig. 2, near the $5d7d\ ^1D_2$ perturber. (b) is from an energy range adjacent to the perturber, i.e., region 2 of Fig. 2. Gaussian intensity masks are used to filter out portions of the Stark maps outside of the respective energy regions.

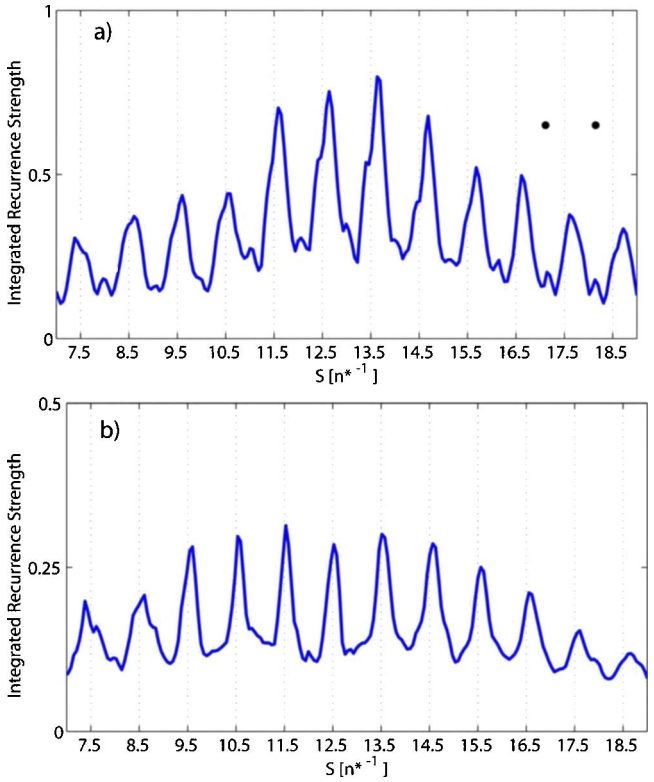

FIG. 10. (Color online) Integrated first-recurrence sequence in Ca from two different energy windows. (a) is taken from region 1 of Fig. 3. (b) is sampled in region 2 of Fig. 3. Gaussian intensity masks are used to filter out portions of the Stark maps outside of the respective energy regions. The $3d3d\ ^1D_2$ perturber strongly affects the d states in region 1, but only weakly influences those in region 2. Bullets (●) mark the predicted positions of recurrence peaks for $S=13.5$ and 14.5, assuming a proportional increase in the Kepler recurrences, as is seen in the zero-field case (see Fig. 4).

range of energies and electric fields that are available in our Stark maps to explicitly examine the dynamical effects of doubly excited perturbers on Stark dynamics. We compare recurrence spectra that cover the same range of scaled energies ϵ but are constructed from different energy windows (see Figs. 2 and 3) that are either very strongly or not very strongly influenced by the Ba and Ca perturbers. Specifically, we focus on the ϵ-integrated recurrence strengths (see Figs. 7 and 8) within the first sequences of Stark returns as shown in Figs. 9 and 10.

Note that for both Ba and Ca, the integrated recurrence spectra generated from energy regions outside of the perturber [Figs. 9(b) and 10(b)] are indistinguishable from single-electron spectra, exhibiting recurrence peaks at, or very near, half-integer values of S with little or no fine-structure or asymmetric broadening. Conversely, spectra generated from localized energy regions surrounding [Fig. 9(a)] or within [Fig. 10(a)] perturbing resonances show dynamical behavior that is distinctly different from that observed in one-electron systems.

At energies near the $5d7d\ ^1D_2$ resonance in Ba, many of the primary Kepler recurrences in sequence 1 are split into two peaks, one centered at half-integer action and the other shifted by 0.28 Kepler periods to larger action. The splitting is insensitive to the precise values of E_0 and ΔE included in the Fourier transform. We can use the wave-packet picture presented above to understand the source of the recurrence fine structure and learn from it.

As noted above, an electron launched from the nucleus as a Rydberg d wave can leave immediately or scatter into a perturbing configuration. For the case of Fig. 9(a), the excitation bandwidth is comparable to the perturber lifetime. Therefore, the initial wave packet has both outgoing Rydberg wave and perturber character. The Rydberg part leaves the nucleus and, because of angular momentum precession in the Stark field, the probability that it will return to the ion core as a d wave decreases but then revives after one Stark period. This direct trajectory reflects purely single-electron dynamics. Accordingly, recurrence peaks are observed at half-integer action during the first Stark sequence. On the other hand, the perturber portion of the wave packet must first scatter back into a Rydberg d wave before it begins its Stark precession. This scattering is characterized by an exponential decay out of the doubly excited state, with a lifetime τ_{AI} ~ 0.6 psec [9], i.e., $\simeq 0.28$ Kepler periods near the center of the perturber at $n*=24.2$. Moreover, because the duration of the effective excitation is comparable to τ_{AI}, electron amplitude transferred into the pertuber configuration at early times will scatter back into Rydberg states and interfere with direct Rydberg excitation at later times. When a Rydberg d wave

returns to the ion core, a portion of it again scatters into, and decays out of, the perturber configuration. This leads to further interferences and additional spatial structure in the Rydberg wave packet [21]. The complexity of the wave packet grows upon each d-wave return to the nucleus.

The splitting, $\Delta S=0.28$, observed in the Ba recurrence peaks is essentially identical to the lifetime of the $5d7d$ perturber [9]. It is, therefore, tempting to associate the first member in each pair of recurrence peaks with direct trajectories, in which the electron remains in the Rydberg channel, and the second peak with indirect trajectories, in which the electron scatters into the perturber configuration for precisely one lifetime and then returns to the Rydberg channel. However, simulations of recurrence spectra from the perturbed Rydberg series in zero field suggests that the fine structure we observe does not provide a direct quantitative measure of the doubly excited lifetime, τ_{AI}. Instead the splitting reflects the interference of electron waves following direct (always Rydberg) and indirect (through the perturber) paths. During the first return of the electron to the nucleus, one expects strong destructive interference in the recurrence signal when the amplitudes for finding an electron near the core via the direct and indirect paths have similar magnitudes but a π-phase difference. The splitting ΔS caused by this interference depends on both the doubly excited lifetime τ_{AI}, and the temporal resolution of the recurrence spectrum. Because the widths of the primary recurrence peaks decrease with increasing ΔE, the dip in the recurrence strength associated with this destructive interference should narrow and move toward smaller S. This analysis suggests that the striking agreement between the observed ΔS and the predicted τ_{AI} is probably fortuitous.

Interestingly, due to experimental energy uncertainties and variations in quantum defects that are not associated with the $5d7d\ ^1D_2$ perturber, the widths of the recurrence peaks in our Ba spectra are quite insensitive to the energy range used in the Fourier transform (compare Figs. 7 and 9). However, as more Rydberg states that are not coupled to the perturber are included, the probability of following the direct, rather than indirect, path around the nucleus increases. As a result, the visibility of the interference minima and the secondary recurrence peaks decrease, but the locations of the minima do not change appreciably.

Another key bit of dynamical information can be gleaned from the experimental recurrence spectra. Simulations of electron dynamics in perturbed Rydberg series clearly show that interferences between direct and indirect paths add complexity to the wave packet upon each return to the nucleus [21]. Thus, the relative simplicity of the recurrence peak fine structure that we observe after one Stark period, i.e., two relatively sharp peaks separated by a single interference minimum, indicates that following the initial launch of the wave packet, there is rapidly diminishing probability for the Rydberg electron to scatter into the perturber configuration until the electron has completed an entire Stark precession. This inference agrees with conclusions drawn by Bates *et al.* in their investigation of Stark dynamics via direct excitation of the $5d7d$ perturber [9].

As a last point in our discussion of Ba, we consider the characteristics of the absorption maps that are responsible for the dynamical features revealed in the recurrence spectra. In the Ba Stark map, the only obvious signature of the $5d7d$ perturber is the dip in the absorption probability near the $6s27d$ state. However, a window resonance in an otherwise uniform Rydberg series (see Fig. 1) cannot cause the recurrence fine structure that we observe. The scaled-recurrence spectrum $R'(S)$ for such a perturbed series is the square of the difference between the Fourier transform of the uniform Rydberg series (a series of narrow recurrences at integer action) and the Fourier transform of an identical spectrum with a Lorentzian amplitude mask centered on the perturber (a series of broad symmetric recurrences at integer action). Thus, $R'(S)$ exhibits a series of narrow recurrence peaks, *symmetrically* broadened at their base, with narrow minima on both sides of the primary peaks. Without the energy variation in the quantum defects, imperceptible in a qualitative viewing of our Ba Stark map, the asymmetric splitting and broadening that we observe would not be present.

For Ca we can follow the same analysis used for Ba. The key difference for the Ca measurements is that the broad perturbing resonance extends to energies beyond those available in the absorption spectra. Thus, over the range of energies where scattering into the perturber is possible, the duration of the effective wave-packet excitation is greater than the perturber lifetime, $\tau_{AI}\simeq 100$ fs. Rydberg waves launched at these energies have a large probability of scattering into the perturber and back out again before the end of the excitation. Immediately following the excitation, the wave packet is primarily an outgoing Rydberg wave that has followed the indirect path. As a result, its evolution has been delayed by a time τ_{AI}, roughly 4% of a Kepler period, as it leaves the nucleus. As in Ba, Stark precession precludes further significant scattering into the perturber configuration for a full Stark period. Accordingly, the ϵ-integrated recurrence strengths at the first Stark return [see Figs. 8 and 10(b)) exhibit primary recurrence peaks that are shifted by roughly 4% relative to the single-electron case [see Fig. 10(a)]. Close inspection of Figs. 8 and 10(b) show that interferences between direct and indirect trajectories, analogous to those observed in Ba, are also seen on the rising edge of the recurrence peaks in Ca. However, these are less obvious due to the relatively small probability that an electron follows the direct path, the short time difference between the direct and indirect paths, and the temporal resolution that is obtained from the limited energy range of the absorption measurements.

For the Ca Stark map, in contrast to Ba, the changes in the d-state quantum defects are probably more apparent than the decrease in absorption probability over the broad perturber resonance. Nevertheless, as in Ba, both spectral effects are important to the underlying dynamics. Through SERS we can clearly identify similar two-electron behavior for the two atoms, albeit on different time scales, in spite of the fact that different signatures of configuration interaction dominate the respective Stark maps.

VI. SUMMARY

We have measured Ca and Ba photoabsorption spectra as functions of energy and static electric-field strength, and

used these to obtain scaled-energy recurrence maps as functions of scaled-energy ϵ and action S. We take advantage of the continuous nature of the recurrence maps to view the ϵ-integrated recurrence strength at the first Stark revival. For each species, we construct this ϵ-independent view of the first return of the electron to the ion core using perturbed and unperturbed spectral regions of the Stark maps, respectively. By direct comparison of these, we are able to clearly identify the dynamical effects associated with electron-electron interaction. In spite of the fact that the frequency-domain absorption spectra have very different appearances, we find that a common picture for the two-electron dynamics in Ba and Ca can be obtained from the recurrence spectra. Similar methods should be applicable for exploring the time-dependent interactions associated with isolated series perturbations in other atoms and molecules as well.

ACKNOWLEDGMENT

This research is supported by the National Science Foundation.

[1] U. Eichmann, K. Richter, D. Wintgen, and W. Sandner, Phys. Rev. Lett. **61**, 2438 (1988).
[2] J. Gao and J. B. Delos, Phys. Rev. A **49**, 869 (1994); A. D. Peters, C. Jaffe, and J. B. Delos, Phys. Rev. Lett. **73**, 2825 (1994).
[3] P. A. Dando, T. S. Monteiro, and S. M. Owen, Phys. Rev. Lett. **80**, 2797 (1998).
[4] F. Robicheaux and J. Shaw, Phys. Rev. A **58**, 1043 (1998); J. A. Shaw and F. Robicheaux, *ibid.* **58**, 1910 (1998).
[5] B. E. Granger and C. H. Greene, Phys. Rev. A **62**, 012511 (2000).
[6] S. N. Pisharody, J. G. Zeibel, and R. R. Jones, Phys. Rev. A **61**, 063405 (2000).
[7] M. Courtney, N. Spellmeyer, H. Jiao, and D. Kleppner, Phys. Rev. A **51**, 3604 (1995); M. Courtney, H. Jiao, N. Spellmeyer, and D. Kleppner, Phys. Rev. Lett. **73**, 1340 (1994); M. Courtney, H. Jiao, N. Spellmeyer, D. Kleppner, J. Gao, and J. B. Delos, *ibid.* **74**, 1538 (1994).
[8] A. Kips, W. Vassen, and W. Hogervorst, Phys. Rev. A **59**, 2948 (1999); G. J. Kuik, A. Kips, W. Vassen, and W. Hogervorst, J. Phys. B **29**, 2159 (1996); A. Kips, W. Vassen, W. Hogervorst, and P. A. Dando, Phys. Rev. A **58**, 3043 (1998).
[9] K. A. Bates, J. Masae, C. Vasilescu, and D. Schumacher, Phys. Rev. A **64**, 033409 (2001).
[10] M. Keeler and T. J. Morgan, Phys. Rev. Lett. **80**, 5726 (1998); M. L. Keeler and T. J. Morgan, Phys. Rev. A **59**, 4559 (1999).
[11] M. L. Keeler, H. Flores-Rueda, J. D. Wright, and T. J. Morgan, J. Phys. B **37**, 809 (2004).
[12] R. V. Jensen, H. Flores-Rueda, J. D. Wright, M. L. Keeler, and T. J. Morgan, Phys. Rev. A **62**, 053410 (2000).
[13] X. J. Liu, J. W. Cao, M. S. Zhan, and J. P. Connerade, J. Phys. B **34**, 1175 (2001); M. S. Zhan, X. J. Liu, J. W. Cao, and J. P. Connerade, *ibid.* **35**, 2069 (2002).
[14] J. A. Armstrong, P. Esherick, and J. J. Wynne, Phys. Rev. A **15**, 180 (1977).
[15] M. Born, *The Mechanics of the Atom* (Frederick Ungar Publishing Co., New York, 1960).
[16] B. J. Lyons, D. W. Schumacher, D. I. Duncan, R. R. Jones, and T. F. Gallagher, Phys. Rev. A **57**, 3712 (1998).
[17] M. Aymar and O. Robaux, J. Phys. B **12**, 531 (1979).
[18] F. Robicheaux, C. Wesdorp, and L. D. Noordam, Phys. Rev. A **60**, 1420 (1999); W. Sandner, K. A. Safinya, and T. F. Gallagher, *ibid.* **33**, 1008 (1986).
[19] T. F. Gallagher, *Rydberg Atoms*, 1st ed. (Cambridge University Press, Cambridge, 1994).
[20] R. R. Jones and L. D. Noordam, Adv. At., Mol., Opt. Phys. **38**, 1 (1997), and references therein.
[21] W. A. Henle, H. Ritsch, and P. Zoller, Phys. Rev. A **36**, 683 (1987).